Available online at www.sciencedirect.com
ScienceDirect
Journal of Power Sources 177 (2008) 386–392
JOURNAL OF POWER SOURCES
www.elsevier.com/locate/jpowsour

Catalyst failure analysis of a direct methanol fuel cell membrane electrode assembly

Zhen-Bo Wang [a,*], Harry Rivera [b], Xin-Peng Wang [c], Hong-Xin Zhang [c], Peter-Xian Feng [c], Emily A. Lewis [d], Eugene S. Smotkin [d,e,**]

[a] *Department of Applied Chemistry, Harbin Institute of Technology, No. 92 West Da-Zhi Street, Harbin 150001, China*
[b] *Department of Chemistry, University of Puerto Rico, Rio Piedras Campus, San Juan, PR 00931, USA*
[c] *Department of Physics, University of Puerto Rico, P.O. Box 23343, San Juan, PR 00931, USA*
[d] *Department of Chemistry and Chemical Biology, Northeastern University, Boston, MA 02115, USA*
[e] *NuVant Systems Inc., Crown Point, IN 46307, USA*

Received 4 October 2007; received in revised form 16 November 2007; accepted 16 November 2007
Available online 10 January 2008

Abstract

Lifetime testing of a single cell direct methanol fuel cell (DMFC) was carried out at 100 mA cm^{-2}, ambient pressure and 60 °C. X-ray diffraction (XRD) and X-ray photoelectron spectra (XPS) were used to characterize the anode and cathode catalysts before and after lifetime testing. The XRD results showed that the particle sizes and lattice parameters of anode catalyst increased from 2.8 to 3.2 nm and from 3.8761 to 3.8871 Å; the cathode catalyst increased from 7.3 to 8.9 nm and from 3.9188 to 3.9204 Å before and after the lifetime test, respectively. The XPS results indicated that during the lifetime period, the extent of oxidation of the anode Pt and Ru components increased, and Ru appears in the XPS of the cathode. Polarization curves, power density curves, and in situ cyclic voltammetry were employed to test the performance of fuel cell and electrochemically active specific surface areas (S_{EAS}) of the anode and cathode catalysts before and after the lifetime test. The overall findings are that the cathode suffers the greatest degradation over the test period and that subtle changes at the anode can have substantial adverse effects on the cathode.

Keywords: Direct methanol fuel cell; Lifetime test; Catalyst degradation; Electrochemically active specific area; In situ cyclic voltammetry

1. Introduction

The direct oxidation of aqueous methanol at the fuel cell anode obviates the need for reformers and humidifiers. This enables a substantial reduction of the fuel cell system weight and complexity [1]. Advancements required for commercialization include improvements in (i) electrocatalyst activity and stability, (ii) membrane resistance to methanol crossover, (iii) water and heat management, and (iv) the durability of the polymer electrolyte membrane. The performance of direct methanol fuel cells (DMFCs) has improved markedly over the last decade due to improvements in catalyst and membrane electrode assembly (MEA) fabrication methods, an area thoroughly reviewed by Gottesfeld and Zawodzinski [2]. Nevertheless, today there are still daunting lifetime degradation processes that must be mitigated. The performance degradation rates of DMFC, generally higher than that of hydrogen PEMFCs, are typically in the range of 10–25 μV h^{-1} [3]. DMFC commercialization demands stable operation for at least thousands of hours (e.g. 5000 h), while fuel cell vehicles and residential power generators require 40,000 h, which is difficult to achieve [4]. MEA failure mechanisms include the growth of catalyst particles, corrosion of catalyst particles resulting in compositional changes, poisoning of electrocatalysts by accumulated intermediates from methanol electro-oxidation or impurities, aging of polymer electrolyte membranes, and changes in the hydrophobic/hydrophilic properties of catalyst and diffusion layers [5–10]. The DMFC cathode operates in a highly corrosive environment due to the high water content, low pH (<1), high temperature (50–90 °C), and high potentials (0.6–1.2 V) coupled with substantial oxygen partial

* Corresponding author. Tel.: +86 451 86417853; fax: +86 451 86413707.
** Corresponding author. Tel.: +1 617 373 7526; fax: +1 617 373 8795.
E-mail addresses: wangzhenbo1008@yahoo.com.cn (Z.-B. Wang), e.smotkin@neu.edu (E.S. Smotkin).

0378-7753/$ – see front matter © 2007 Elsevier B.V. All rights reserved.
doi:10.1016/j.jpowsour.2007.11.070

pressures. This renders both the catalysts and carbon supports vulnerable to a host of degradation mechanisms. The loss of activity at the cathode can result from a loss of dispersion, long term poisoning of the catalyst, or a combination of both [7,10]. With respect to dispersion, two mechanisms for particle size growth are Ostwald ripening and coalescence [11–15]. Although coalescence has been reported to be insignificant for carbon-supported catalysts at temperatures below 500 °C in the gas phase [12], this may not be the case with DMFCs where metal black catalysts are typically used. The primary growth mechanism, Ostwald ripening, would be expected to be more serious at the cathode, because of the proximity of the catalyst potential to the Pourbaix corrosion boundary [14]. Others have reported that the agglomeration of catalysts at the anode may be underestimated because methanol may be more corrosive than water in an operating DMFC [16]. There have been a number of reports of Ru dissolution and crossover from the anode as well [8,10]. In this work, we carried out a 110 h lifetime test in a DMFC single cell at 60 °C using Johnson Matthey unsupported Pt and PtRu catalysts. The MEA catalytic layers were characterized by electrochemical, X-ray diffraction (XRD), and X-ray photoelectron spectra (XPS) prior to and after the lifetime study.

2. Experimental

2.1. MEA preparation

MEAs were prepared as previously described [17–19]. Briefly, Johnson Matthey Pt black and PtRu black were used at the cathode and anode, respectively. The PtRu black and 5 wt% Nafion solution (E.I. DuPont De Nemours & Co.) were mixed in isopropanol solution to form a dispersion of catalyst black ink. The cathode catalyst ink was prepared similarly with Pt black, although PTFE dispersion was included in the ink. The inks were deposited onto the GDLs by paint brush at loading of 4 mg cm^{-2} for both electrodes. The carbon cloth (E-TEK, ELAT/NC/DS/V2 double sided ELAT electrode, carbon only, no metal, 20% wet proofed) was used as the gas diffusion layer (GDL) and backing layer in the cathode. The carbon paper (Toray paper TGPH 060) was used as the anode GDL. DuPont Nafion 117 membrane was use as the electrolyte membrane. The Nafion membrane was pretreated by dilute nitric acid (nitric acid:deionized water of 18 MΩ cm (nanopure water) with a volume of 1:1) at boiling temperature for 20 min and then rinsed 5 times with nanopure water. The Nafion membrane was then immersed in boiling nanopure water for 1 h. The MEA was formed by hot-pressing the anode and cathode diffusion layers onto the Nafion film.

2.2. Electrochemical measurements

2.2.1. Single fuel cell tests

Single fuel cell data were acquired at 60 °C using a 5 cm^2 active area fuel cell (NuVant System Inc., Crown Point, IN). Fig. 1 schematizes the experimental setup for fuel cell testing and in situ cyclic voltammetry (CV) measurements. Methanol (1 mol L^{-1}) was delivered to the anode at 2.5 mL min^{-1} with no back pressure, while dry air was delivered to the cathode at 100 mL min^{-1} at ambient pressure. The polarization curves, power density curves, and potential–time curve were obtained using a load unit (Series 890B, Scribner Associates Inc., Southern Pines, NC, USA) with a 4 V d.c. unregulated power supply in series [17] with the fuel cell. The potential–time curve was measured in galvanostatic mode with a current density of 100 mA cm^{-2} for 110 h. The fuel cell was conditioned with nanopure water at the anode and air at 60 °C at the cathode for 5 h. After conditioning, nanopure water was replaced with aqueous methanol for 24 h in galvanostatic mode at 10 mA cm^{-2} prior to the acquisition of lifetime data.

2.2.2. Cyclic voltammetry

CVs were obtained using a PAR potentiostat/galvanostat (EG&G Model 273A) at 25 °C. The electrochemically active specific surface area (S_{EAS}) of the anode and cathode catalysts was determined by CO-stripping and hydrogen desorption measurements, respectively. For CO-stripping, the fuel cell cathode side was set up for use as both a dynamic hydrogen electrode (DHE) and counter electrode by first purging the cathode with nitrogen for 10 min and then switching to humidified hydrogen

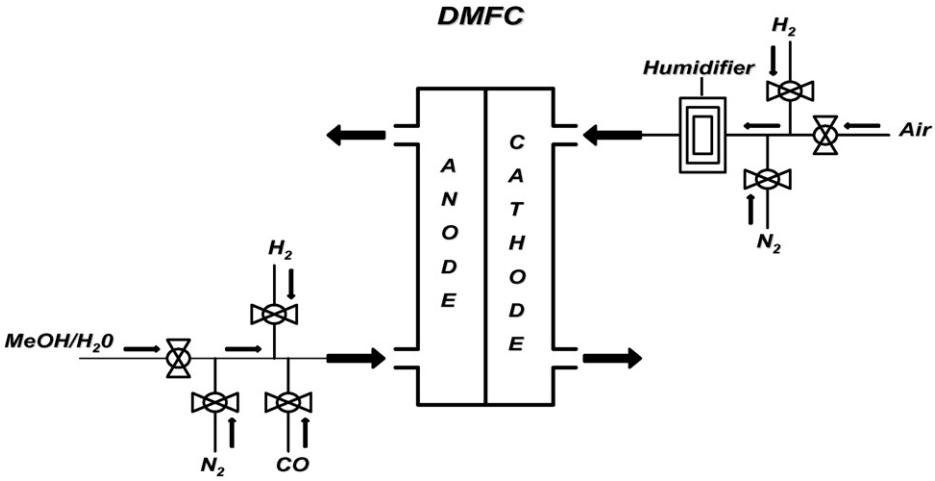

Fig. 1. Schematic of fuel cell test system. Fuel and oxidant flow in counter directions.

at 100 mL min^{-1} and ambient pressure. The anode was then purged with nitrogen for 10 min, replaced with CO for 15 min, and purged again with nitrogen for 10 min. The potential was scanned (0.02 V s^{-1}) between 0.05 and 1.2 V. The integrated peak area of CO electro-oxidation was used to calculate the S_{EAS} of the anode. For the hydrogen desorption analysis at the cathode, the anode served as reference and counter electrode, as described above. The cathode was purged with humidified nitrogen for 10 min. The CV curve was recorded within the potential range of 0.05–1.2 V at 0.02 V s^{-1}. All potentials are reported versus DHE.

2.3. Characterization of physical properties

After electrochemical testing, the MEA was carefully removed from the cell. The anode and cathode GDLs were separated from the MEA and cut into smaller pieces for subsequent analysis by XRD and XPS.

2.3.1. X-ray diffraction

XRD measurements on the catalyzed GDL were recorded on a Rigaku Ultima III X-ray diffractometer system (Rigaku MSC, Woodlands, TX) using a graphite crystal counter monochromator that filtered Cu Kβ radiation. The X-ray source was operated at 40 kV and 40 mA. The patterns, recorded in the 2θ range of 20–140°, were obtained using high precision and high resolution parallel beam geometry in the step scanning mode at 1 deg min^{-1}. The identification of phases was made by referring to the Joint Committee on Powder Diffraction Standards International Center for Diffraction Data (JCPDS-ICDD) database. Lattice parameters and crystallite sizes were calculated using JADE 7 Plus software (Rigaku). Grain sizes were determined from the Scherrer equation using the Pseudo-Voigt profile function.

2.3.2. X-ray photoelectron spectrometry

The XPS study of surface composition involved a special X-ray photoelectron spectrometer (VG ESCALAB MKII) with the Al Kα X-ray source of 1486.6 eV, which recorded the spectra from the 45° take-off angle at the chamber pressure below 5×10^{-9} Pa. The C 1s electron binding energy was referenced at 284.6 eV, and a nonlinear least squares curve-fitting program was employed with a Gaussian–Lorentzian production function [20,21]. The deconvolution of the XPS spectra was achieved with the reported procedures [22–26].

3. Results and discussion

Fig. 2 shows the degradation of the fuel cell potential operated galvanostatically with time at 60 °C at 100 mA cm^{-2}. The periodic performance recovery corresponds to refilling of the methanol solution.

This short-term recovery process, superimposed upon a long-term non-recoverable process, is related to a positive potential excursion that occurs during fuel starvation. The mass transport overpotential is accommodated by a positive shift of the potential. The recovery process may be attributed to the reestablishment of equilibrium among the ruthenium oxides [27,28],

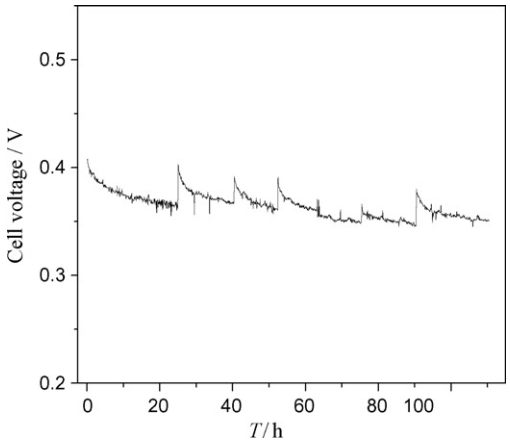

Fig. 2. Single cell (active area 5 cm^2) performance at 60 °C, 100 mA cm^{-2} over 100+ h. Anode: PtRu black, 4 mg cm^{-2}. Cathode: Pt black, 4 mg cm^{-2}. Anode: 1.0 mol L^{-1} CH_3OH at 2.5 mL min^{-1}. Cathode: dry air at ambient pressure, 100 mL min^{-1}.

or possibly the oxidative removal of poisoning adsorbates. The irrecoverable loss may be related to the degradation of catalysts, the dissolution of Nafion solution in catalysts layer [29], and/or the aging of polymer electrolyte membrane [9]. The short-term recoverable loss illustrated in Fig. 2 is to be differentiated from that reported by Eickes and Zelenay [7,8]. They elucidated a short-term loss due to oxide formation at the cathode. Recovery was accomplished by air starvation, which causes a negative shift of the cathode potential that removes the oxide layer. In our case (Fig. 2), recovery occurs by an anodic shift of the anode electrode. Thus there are short-term recovery issues at both the anode and the cathode sides of the DMFC.

Cell performance and power density curves at 60 °C were obtained before and after lifetime testing (Fig. 3). The maximum power density drops from 72.3 to 42.4 mW cm^{-2} (i.e. a 41.3% loss). The loss of power density at cell voltage of 0.4 V is about 50.5%.

The comparative CO-stripping waves before and after the lifetime test (Fig. 4) show that within the time period studied, the changes at the anode are at most, subtle. Fig. 5 shows the hydrogen desorption waves of the cathode catalyst before and after the lifetime test. It is immediately obvious that reduction of

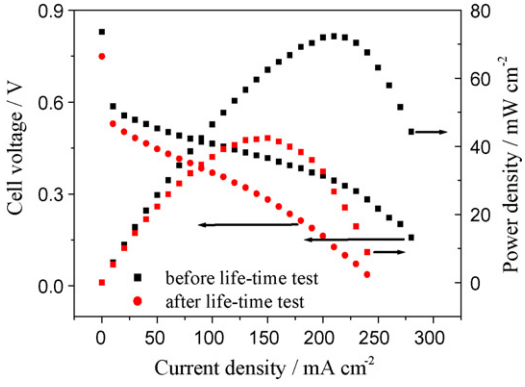

Fig. 3. DMFC single cell before and after the lifetime test. Temperature: 60 °C. Anode feed: 1 mol L^{-1} CH_3OH solution; flow rate: 2.5 mL min^{-1}. Cathode feed: air at ambient pressure; flow rate: 100 mL min^{-1}.

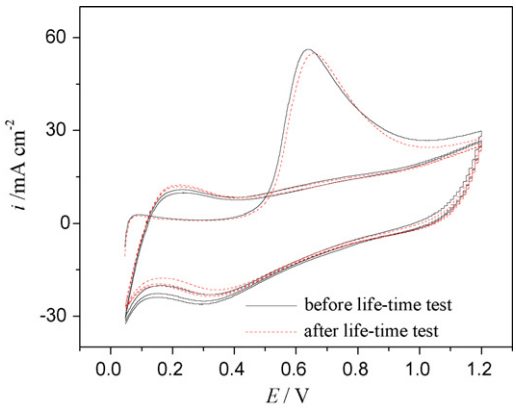

Fig. 4. CO-stripping (25 °C) at the anode before and after lifetime test.

Table 1
The different parameters of the anode and cathode catalysts before and after the lifetime test

Catalysts	Anode		Cathode	
	Before	After	Before	After
CO oxidation peak potential (V)	0.634	0.654	–	–
CO oxidation onset potential (V)	0.508	0.522	–	–
S_{EAS} ($m^2\ g^{-1}$)	35.83	33.56	11.19	4.65
Relative change of S_{EAS} (%)	6.30		58.40	
d_{XRD}	2.8	3.2	7.3	8.9
Relative change of d_{XRD} (%)	14.30		21.90	
S_{XRD}	109.9	96.2	38.4	31.5
Relative change of S_{XRD} (%)	12.50		18.00	
Catalyst utilization (%)	32.60	34.90	29.10	14.50
Lattice parameters (Å)	3.8761	3.8871	3.9188	3.9204

the hydrogen desorption wave integral is accompanied by a loss of the characteristic Pt crystallographic face dependent adsorption waves, and an increase in the double layer capacitance of the electrode. Such high double layer capacitance is typical for PtRu electrodes. Ru crossover and plating onto the cathode has been previously reported [10]. Note the presence of a peak around 0.64 V at the beginning scan. The unknown peak is organic contaminant from the Nafion solution. On consecutive scans, the unknown peak disappears.

The electrochemically active specific area (S_{EAS}), which reflects the intrinsic electrocatalytic activity of a catalyst, is calculated with the recognized method based on the curves of CO-stripping voltammetry and hydrogen adsorption–desorption curve [30,31], respectively, through the following equation:

$$S_{EAS} = \frac{Q_1}{GQ_2} \quad (1)$$

where Q_1 is the charge quantity calculated from integrated in CV curves for CO desorption electro-oxidation or hydrogen adsorption–desorption in micro coulomb (μC), Q_2 is the charge required to oxidize a monolayer of CO on alloy catalyst of 420 (μC cm^{-2}) [32] or single layer saturation coverage hydrogen on Pt surface area of 210 (μC cm^{-2}) [31], and G represents the total metal loading (mg) in the electrode.

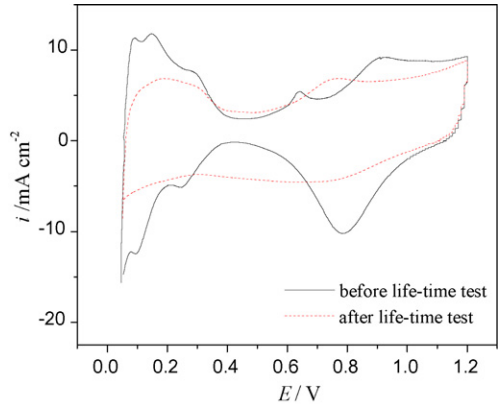

Fig. 5. Hydrogen desorption test of cathode catalyst before and after the lifetime test. Temperature: 25 °C.

The S_{EAS} calculations are presented in Table 1. Anode S_{EAS} suffer a small change of 2.27% while the cathode show a 58.4% change. These noticeably reduce the 'triple-phase boundaries' where the electrolyte, reaction material, and electrically connected catalyst particles contact together. These results point out that the Pt black catalyst and catalyst layer in the cathode electrode were already decayed. Based on this, we can say

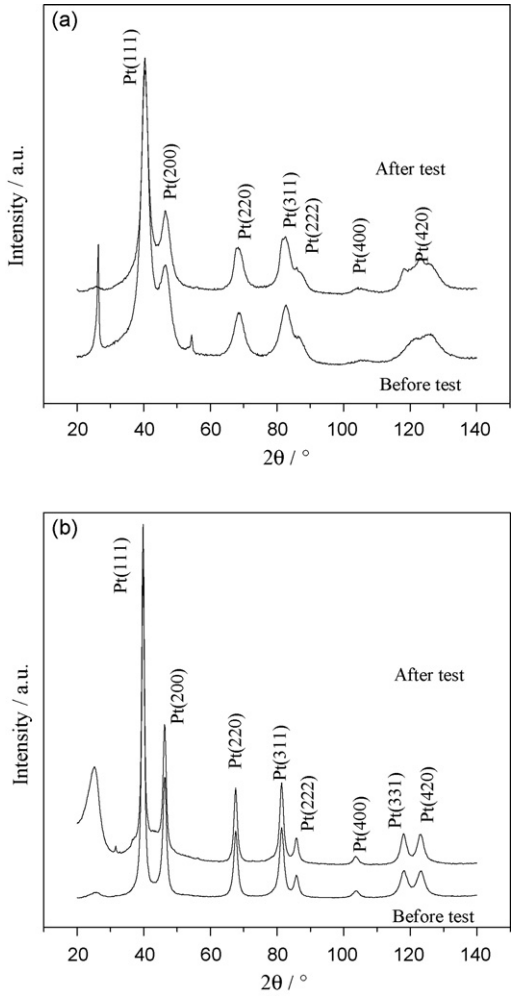

Fig. 6. XRD patterns of (a) anode catalyst and (b) cathode catalyst.

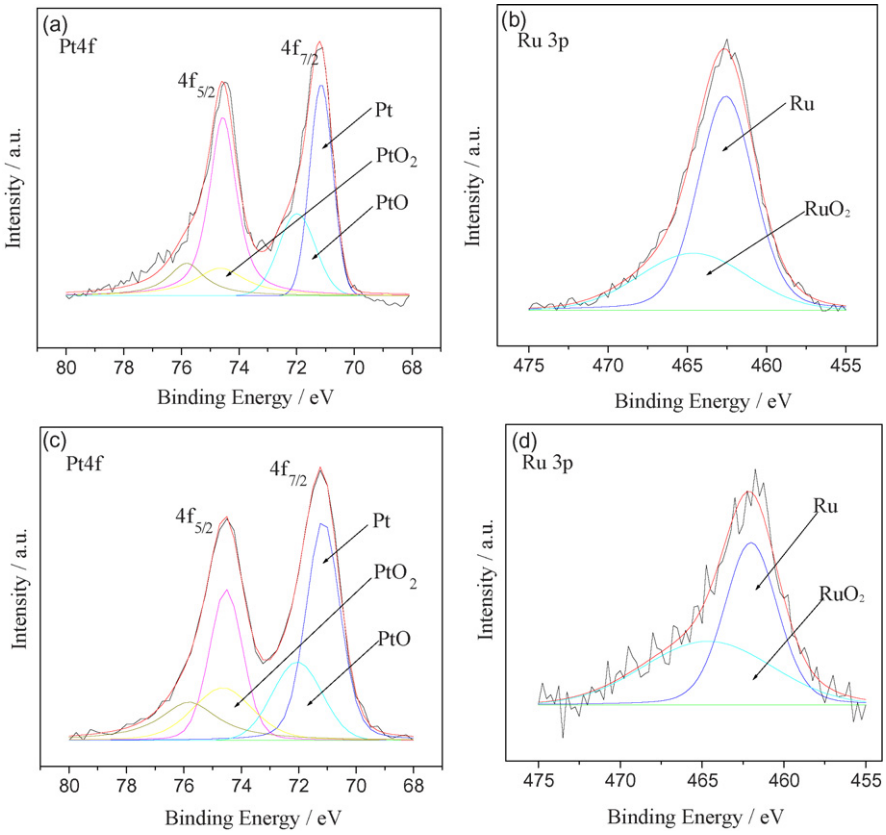

Fig. 7. XPS core level spectra of anode catalyst (a and b) before and (c and d) after the lifetime test.

that DMFC performance degradation can be attributed to all the changes that occurred on the cathode catalyst. Also the utilizations (S_{EAS}/S_{XRD}) of catalysts in both electrodes are almost the same, about 30% before the lifetime test. This result is in agreement with the reports in the literature [9,33]. After the lifetime test, the utilization of anode catalyst slightly increases to 34.9%. This is probably a result of a prolonged conditioning period of the anode during the lifetime testing. However, the utilization of cathode catalyst severely decreases to 14.5%.

After the single cell test, the used MEA was separated and segmented into samples for further analysis. XRD patterns of anode and cathode were measured (Fig. 6). The observed diffraction peaks at 26° in the anode and cathode are attributed to the hexagonal graphite structures (0 0 2) in carbon black remaining on the catalyst layer after peeling off the GDLs. The Pt and PtRu black forms a face centered cubic (fcc) structure and has major peaks of (1 1 1), (2 0 0), (2 2 0), (3 1 1), (2 2 2), and (4 0 0). The mean particle sizes and lattice parameters of catalysts before and after the lifetime test were calculated from XRD patterns by using JADE software and are listed in Table 1.

Table 1 shows that changes in the particle size and lattice parameters of anode catalyst are minimal. However, the cathode catalyst experiences a particle size change of almost 2 nm, and no significant changes on the lattice parameters in agreement with Xin and co-workers [9]. As mentioned earlier, Ostwald ripening would be expected to occur to a greater extent at the cathode than at the anode so it is not surprising that loss of dispersion at the cathode is more substantial. The relative effects of coalescence and Ostwald ripening are still an open question [14]. Table 1 shows that the lattice parameter of the PtRu alloy catalyst increases slightly, presumably due to the oxidation, dissolution, and separation of Ru metal atoms in the Pt crystalline

Table 2
Oxide content of Pt and Ru in the anode and cathode before and after lifetime test

	Electrodes									
	Anode					Cathode				
	Pt/Oxide concentrations (%)[a]			Ru/Oxide concentrations (%)[a]		Pt/Oxide concentrations (%)[a]			Ru/Oxide concentrations (%)[a]	
	Pt	PtO	PtO_2	Ru	RuO_2	Pt	PtO	PtO_2	Ru	RuO_2
Pre-lifetime test (%)	62.0	28.3	9.7	68.4	31.6	64.9	26.0	9.1	–	–
Post-lifetime test (%)	55.9	29.4	14.7	53.8	46.2	53.2	29.3	17.5	12.8	87.2

[a] Oxide distribution.

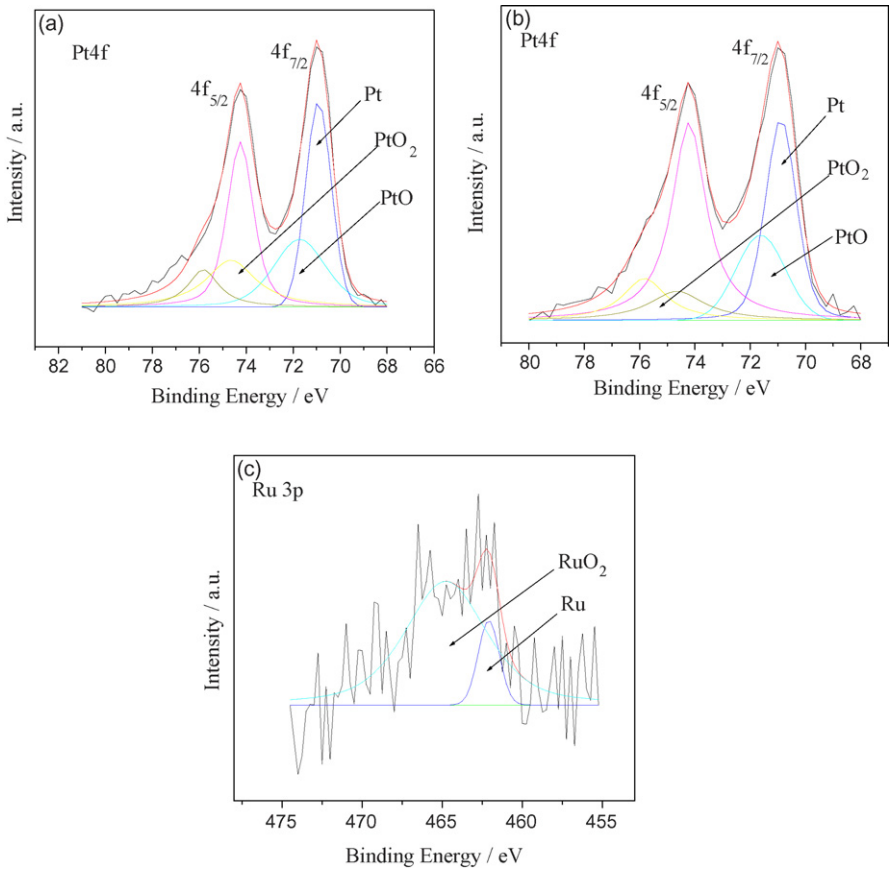

Fig. 8. XPS core level spectra of cathode catalyst (a) before and (b and c) after the lifetime test.

lattices. However the CO-stripping waves showed only subtle changes at the surface. The lattice parameter of the cathode did not change much. The implication is that only a small loss of Ru at the anode can result in a large change in performance of the cathode. Although the bulk structure of the cathode is not changing, the surface is substantially poisoned throughout the lifetime test. Fig. 5 suggests that the surface of the Pt cathode is poisoned, most likely by plating of Ru onto the surface. This is consistent with the findings of the Zelenay group [8,10].

The specific surface area of catalysts (denoted as S_{XRD}) calculated from XRD patterns are also listed in Table 1. The change of the ratio of S_{EAS} is slightly smaller than is the S_{XRD} in the anode. However, the change of the ratio of S_{EAS} is much higher than it is S_{XRD} in the cathode. This suggests that the catalyst agglomeration is not the sole reason for the S_{EAS} loss in the cathode. The Nafion may be delaminating from the catalyst particles as the surface morphology changes. This loss of the 'triple-phase boundaries', may contribute to the loss of the S_{EAS}.

Figs. 7 and 8 present the curve-fitted Pt 4f XPS spectra of PtRu black anode catalyst and Pt black cathode catalyst, respectively, before and after the lifetime test.

The oxidation states of Pt, Ru, and their relative amount before and after the lifetime test are listed in Table 2. Table 2 shows that the oxide content of the cathode catalyst is substantially increased after the lifetime test. This is consistent with the proposed mechanism that oxide formation at the cathode is a failure mechanism. The XPS results also show that while the cathode started out as pure Pt, Ru appears as a component of the cathode after the lifetime test. This explains the loss of the Pt crystallographic face dependent hydrogen desorption–adsorption waves in Fig. 5. The Pt metal content in the PtRu black (55.9%) after the lifetime test in anode is only 6.1% lower than that of it (62.0%) before the lifetime test. Also, the total amount of oxidation states (Pt(II) and (IV)) after the lifetime test is a little higher than before the lifetime test, especially the increase of Pt(IV) oxide of 5%. However, the Ru metal content after the lifetime test rapidly decreases, and meanwhile the Ru(IV) oxide content after the lifetime test sharply increases, and its relative amount is 14.6% higher that before the lifetime test. The relative peak area of Pt(II), Pt(IV), and Ru(IV) in the PtRu anode alloy does not change after the stability test. The Ru metal of the PtRu black catalyst during the operation is easily dissolved.

4. Conclusions

After 110 h of operation there was a 41.3% loss at the maximum power point of the fuel cell. Catalyst ripening is more severe at the cathode than at the anode: Ostwald ripening is enhanced at the more positive potentials of the cathode. A small change at the anode can result in substantial changes at the cathode. The Ru from the anode crosses over to the cathode and plates out on the cathode Pt catalyst. The lattice parameter at the cathode remains essentially unchanged, which indicates

that the failure mechanism at the cathode is more of a surface phenomenon rather than a bulk issue (i.e. Ru poisoning of the surface). Pulsed fuel starvation results in recovery of performance when the cell is operated galvanostatically, indicating that the poisoning species can be oxidatively removed. Better recovery methods than fuel pulsing warrant attention.

Acknowledgements

This work was supported by the National Natural Science Foundation of China (grant no. 20606007), the Army Research Office Grant No. W911NF-05-1-0020, and the NASA-UPR Center for Nanoscale Materials grant no. NCC3-1034. Thanks are due to Qiangu Yan of NuVant Systems, and to the reviewers for helpful comments.

References

[1] A.R. Landgrebe, K. Rajat, D.H.W. Sen, Proceedings of the Electrochemical Society 92, vol. 14, 1992, pp. 1–223.
[2] S. Gottesfeld, T.A. Zawodzinski, Advances in Electrochemical Science and Engineering, vol. 5, Wiley-VCH, 1997, pp. 229–244.
[3] S.D. Knights, K.M. Colbow, J. St-Pierre, D.P. Wilkinson, J. Power Sources 127 (2004) 127–134.
[4] S.Y. Ahn, S.J. Shin, H.Y. Ha, S.A. Hong, Y.C. Lee, T.W. Lim, I.H. Oh, J. Power Sources 106 (2002) 295–303.
[5] M.K. Jeon, J.Y. Won, S.O. Kwang, K.R. Lee, S.I. Woo, Electrochim. Acta 53 (2007) 447–452.
[6] P. Waszczuk, A. Wieckowski, P. Zelenay, S. Gottesfeld, C. Coutanceau, J.M. Leger, C.J. Lamy, Electroanal. Chem. 511 (2001) 55–64.
[7] C. Eickes, J.D. Piotr Piela, P.J. Zelenay, Electrochem. Soc. 153 (2006) A171–A178.
[8] P. Zelenay, Y.S. S Kim, Fuel Cells Durability Workshop, Washington, DC, 2005, p. 29.
[9] W. Chen, G. Sun, J. Guo, X. Zhao, S. Yan, J. Tian, S. Tang, Z. Zhou, Q. Xin, Electrochim. Acta 51 (2006) 2391–2399.
[10] P. Piela, C. Eickes, E. Brosha, F. Garzon, P. Zelenay, J. Electrochem. Soc. 151 (2004) A2053–A2059.
[11] P. Ascarelli, V. Contini, R. Giorgi, J. Appl. Phys. 91 (2002) 4556–4561.
[12] J.A. Bett, K. Kinoshita, P. Stonehart, J. Catal. 35 (1974) 307–316.
[13] J.A.S. Bett, K. Kinoshita, P.J. Stonehart, Catalysis 41 (1976) 124–133.
[14] P.J. Ferreira, G.J. la O, Y. Shao-Horn, D. Morgan, R. Makharia, S. Kocha, H.A. Gasteiger, J. Electrochem. Soc. 152 (2005) A2256–A2271.
[15] C.G. Granqvist, R.A. Buhrman, J. Catal. 42 (1976) 477–479.
[16] J. Liu, Z. Zhou, X. Zhao, Q. Xin, G. Sun, B. Yi, Phys. Chem. Chem. Phys. 6 (2004) 134–137.
[17] B. Gurau, E.S. Smotkin, J. Power Sources 112 (2002) 339–352.
[18] S. Stoupin, E.-H. Chung, S. Chattopadhyay, C.U. Segre, E.S. Smotkin, J. Phys. Chem. B 110 (2006) 9932–9938.
[19] E.S. Smotkin, in: S.-G. Sun, P.A. Christensen, A. Wieckowski (Eds.), In Situ Spectroscopic Studies of Adsorption at the Electrode and Electrocatalysis, 1st ed., Elsevier, Oxford, UK, 2007, pp. 247–272.
[20] K.-W. Park, J.-H. Choi, B.-K. Kwon, S.-A. Lee, Y.-E. Sung, H.-Y. Ha, S.-A. Hong, H. Kim, A. Wieckowski, J. Phys. Chem. B 106 (2002) 1869–1877.
[21] C. Bock, C. Paquet, M. Couillard, G.A. Botton, B.R. MacDougall, J. Am. Chem. Soc. 126 (2004) 8028–8037.
[22] F.J. Rodriguez-Nieto, T.Y. Morante-Catacora, C.R. Cabrera, J. Electroanal. Chem. 571 (2004) 15–26.
[23] A.S. Arico, G. Monforte, E. Modica, P.L. Antonucci, V. Antonucci, Electrochem. Commun. 2 (2000) 466–470.
[24] A.K. Shukla, A.S. Arico, K.M. El-Khatib, H. Kim, P.L. Antonucci, V. Antonucci, Appl. Surf. Sci. 137 (1999) 20–29.
[25] Y. Liang, H. Zhang, Z. Tian, X. Zhu, X. Wang, B. Yi, J. Phys. Chem. B 110 (2006) 7828–7834.
[26] Z.-B. Wang, G.-P. Yin, Y.-G. Lin, J. Power Sources 170 (2007) 242–250.
[27] H. Hoster, T. Iwasita, H. Baumgartner, W. Vielstich, J. Electrochem. Soc. 148 (2001) A496–A501.
[28] H. Hoster, T. Iwasita, H. Baumgartner, W. Vielstich, Phys. Chem. Chem. Phys. 3 (2001) 337–346.
[29] G. Gebel, P. Aldebert, M. Pineri, Macromolecules 20 (1987) 1425–1428.
[30] A. Pozio, M. De Francesco, A. Cemmi, F. Cardellini, L. Giorgi, J. Power Sources 105 (2002) 13–19.
[31] C.L. Green, A. Kucernak, J. Phys. Chem. B 106 (2002) 1036–1047.
[32] J. Jiang, A. Kucernak, Chem. Mater. 16 (2004) 1362–1367.
[33] S.C. Thomas, X. Ren, S. Gottesfeld, J. Electrochem. Soc. 146 (1999) 4354–4359.